phys. stat. sol. (b) **232**, No. 1, 134–137 (2002)

The Influence of Many-Body and Bandstructure Effects in the Design of High Power Diode Lasers

M. F. Pereira Jr.[1)*)] (a) and H. Wenzel (b)

(a) Instituto de Física, Universidade Federal da Bahia, 40210-340 Salvador BA, Brazil

(b) Ferdinand–Braun–Institut für Höchstfrequenztechnik, Albert Einstein Str. 11, 12489 Berlin, Germany

(Received November 26, 2001; accepted March 15, 2002)

PACS: 42.55.Px; 73.21.Fg; 78.20.Bh

A microscopic many-body theory is used to compute the dielectric constant of single quantum wells. The nonparabolic electron and hole subband dispersion relations and dipole transition moments of the free propagators stem from the numerical solutions of an 8×8 $\mathbf{k} \cdot \mathbf{p}$ Hamiltonian. The resulting local optical response and carrier recombination rates are used as input for realistic device simulators. Absorption, gain as well as threshold currents of distributed Bragg reflector lasers are presented.

The high wall-plug efficiency and reliability of high-power diode lasers make them extremely relevant for future laser technology applications. As the production methods evolve and technological applications become more demanding, the design and simulation of those devices also evolves. Physical effects previously ignored in the device simulators must be included for realistic prediction of device operation characteristics. Many-particle theories have given a significant impact to the understanding of the microscopic processes responsible for the operation of semiconductor optoelectronic devices, at both, steady state and ultrafast regimes [1–3]. In particular, a recent study has shown the power of many-body theories and their fundamental importance for concrete simulations of a three section distributed Bragg reflector (DBR) laser. The threshold current and external efficiency can not be explained without many-particle corrections [4]. There are, of course, so far no approaches free of approximations, and different techniques have been used to obtain numerical codes, fast enough for systematic computations allowing direct comparison with experiments and containing sufficient predictable power. At high power operation, due to spatial and spectral hole burning, the electron subbands of quantum well (QW) structures are populated in regions of the k-space where their nonparabolicity as well as that of holes can not be neglected. Usually, hole nonparabolicity is taken into account but not that of electron subbands, which are approximated to be parabolic. In this paper we proceed a step with respect to previous publications [4, 5], and include both, hole and electron nonparabolicity in the Green-function approach through the numerical solution of an 8×8 $\mathbf{k} \cdot \mathbf{p}$ Hamiltonian combined with many-body corrections. A generalised Bethe–Salpeter equation that satisfies the Kubo–Martin–Schwinger (KMS) sum rule, which is crucial for understanding certain features of the gain spectra is solved. The resulting local optical re-

[1)] Corresponding author; e-mail: pereira@physik.tu-berlin.de

[*)] Present address: Institut für Theoretische Physik, Technische Universität Berlin, Hardenbergstrasse 36, 10623 Berlin, Germany.

 0370-1972/02/23207-0134 $ 17.50+.50/0

sponse is used as starting point for computation of the modal gain and threshold current characteristics of different structures. The general many-particle theory has been previously explained in detail with the exception of parabolic electron subbands being used [2]. Here we just explain in words the main underlying features of it.

We apply a Keldysh–Green-function approach for carriers (G), photons (D), and plasmons (W) to describe the coupled light-excited semiconductor system [6, 7]. The Keldysh–Green-function time evolution is described by Dyson equations, characterized by free propagators G_0^{-1}, D_0^{-1}, W_0^{-1}, and self-energies: Σ, P, and p, called carrier self-energy, transverse, and longitudinal polarization functions, respectively. Detailed bandstructure and quantum-confinement effects, obtained by solving either the Luttinger Hamiltonian [8], or an 8-band $\mathbf{k} \cdot \mathbf{p}$ Hamiltonian [9], are included in the free-carrier propagator G_0^{-1}, and make the input for the solution of our many-body problem. Each of the self energies change the bare into dressed propagators in a specific way: Σ renormalizes the bandgap and introduces carrier scattering, responsible for dephasing in the polarization function. Plasmon screening of the Coulomb interaction is described by p. The excitation-dependent absorption coefficient α and the refractive index, are obtained from P, which also defines scattering rates (generation/recombination, i.e. absorption/emission) in the photon kinetics. It further includes bound states (excitons) in the photon spectral density. Both P and the carrier self energy Σ can be written as a sum of a RPA term and a Coulomb-correlation contribution, expressed by means of a T-matrix which satisfies the Bethe–Salpeter equation [2],

$$P(1, 1, 2, 2) = G(1, 2)\, G(2, 1) + G(1, 3)\, G(4, 1)\, P(3, 4, 2, 2)\,. \tag{1}$$

In this paper, we consider T-matrix correlations beyond RPA in the spectral density of photons, but restrict the carrier self-energies to RPA, i.e. $\Sigma(1, 2) = G(1, 2)\, W(1, 2)$. The dephasing, responsible for the gain/absorption broadening, is given by the imaginary part of Σ^{r} (spectral information is included in the retarded Keldysh components, superscript $^{\mathrm{r}}$). Here we use a partly phenomenological fit to the full expression [8]. The resulting expressions for the polarization function can be combined with the solutions of the photon Green function propagator which are directly related to the quantum-mechanical Poynting vector and thus lead to light-emission spectra [7]. Using the fact that P satisfies exactly the Kubo–Martin–Schwinger (KMS) relation, we obtain the local absorption and photoluminescence spectra I [2],

$$\alpha(\omega) \sim \frac{c}{2\omega\, \sqrt{\epsilon(\infty)}}\, \mathrm{Im}\, \{P^{\mathrm{r}}(\omega)\}\,, \qquad I(\omega) \sim \frac{\mathrm{Im}\, \{P^{\mathrm{r}}(\omega)\}}{1 - \exp\, (\beta(\hbar\omega - \mu))}\,, \tag{2}$$

where $\mu = \mu_{\mathrm{e}} + \mu_{\mathrm{h}}$ is the total chemical potential (Fermi voltages).

Our modelling of MQW laser characteristics is best illustrated by the following numerical examples. We start by computing bandstructure and oscillator strengths for the non-interacting (free-carrier) problem by solving either a 4-band (Luttinger) or an 8-band $\mathbf{k} \cdot \mathbf{p}$ Hamiltonian [9]. Linear response theory is then used to derive the complex dielectric function, the rate of radiative recombination with either a free carrier or a many-particle approach. The Fermi voltage is then computed selfconsistently with the selfenergy corrections to the free carrier energy levels. Note that the theory is linear in the probe field that is amplified in the medium, but arbitrarily nonlinear in the excess carrier density generated either optically or electronically.

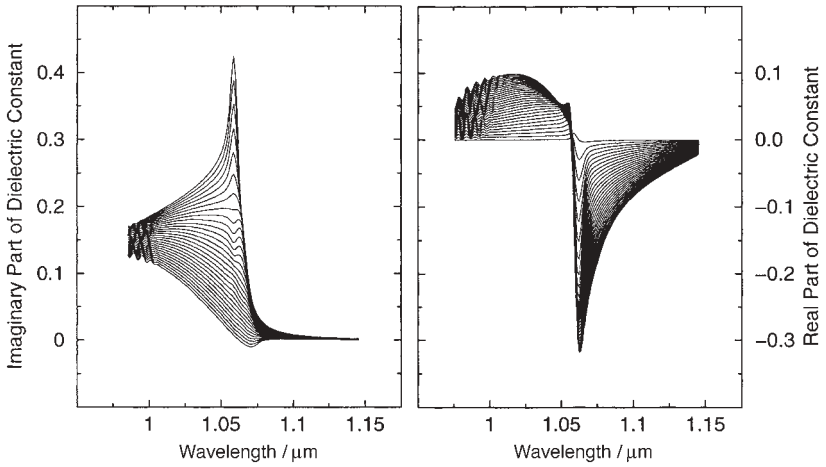

Fig. 1. Imaginary (left) and corresponding real part (right) of the carrier-dependent changes induced in the local dielectric constant computed from a Kramers–Kronig transformation of the difference between the imaginary part for a given density and the linear absorption of the carrier-dependent contribution to the local dielectric constant of a quantum well structure designed to operate at 1.06 μm. The input bandstructure is computed with a 8×8 $\mathbf{k} \cdot \mathbf{p}$ Hamiltonian. Only the E1–HH1 exciton contribution is included. Excitonic bleaching and the development of negative absorption (gain) are clearly depicted as the excess carrier density varies between 0 (linear absorption limit) and 4×10^{18} cm^{-3}

Figure 1 (left) depicts the imaginary part of the carrier-dependent contribution to the local dielectric constant of a quantum well structure designed to operate at 1.06 μm. Only the E1–HH1 exciton contribution is included. Excitonic bleaching and the development of negative absorption (gain) are clearly depicted as the excess carrier density varies between 0 and 4×10^{18} cm^{-3}. The corresponding changes in the real part of the carrier-dependent changes induced in the local dielectric constant computed from a Kramers–Kronig transformation of the difference between the imaginary part for a given density and the linear absorption is given in the right panel of Fig. 1. The resulting structure follows the bleaching of the near bandgap excitonic absorption and the development of optical gain. Waveguiding and drift diffusion of carriers in the transverse plane is taken into account in a device simulator leading to a complex propagation constant, amplified spontaneous emission, and injection currents. Finally, coupled wave theory yields power–voltage–current characteristics and the lasing wavelength spectrum. The threshold current of a three section DBR laser at room temperature operating around 1.0 μm, for different lengths of the phase section in μm is presented in Fig. 2. The active layer consists of of a 10 nm InGaAs–GaAs QW. The longer the phase section, the more light is absorbed before it reaches the DBR where it is reflected and the smaller the interband absorption has to be, meaning that the band gap wavelength must be shifted to longer values. The external voltage in the passive section is zero (unbiased) which corresponds to usual operation conditions.

In summary, the combination of band structure and some many-body effects given in the numerics presented here leads to a realistic device simulation capability experiment and is able to explain features of device operation where a simple free carrier approach fails. It must however be pointed out that several approximations have been used and a

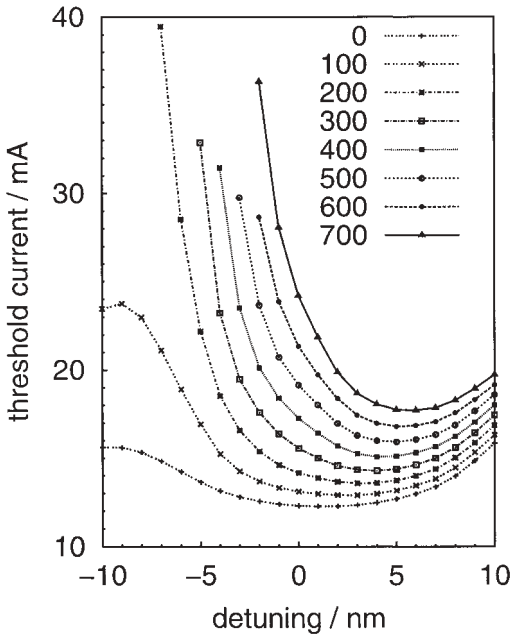

Fig. 2. Threshold current of a three section DBR laser (10 nm InGaAs–GaAs QW) at room temperature operating around 1.0 μm, for different lengths of the phase section in μm. The longer the phase section, the more light is absorbed before it reaches the DBR where it is reflected and the smaller must be the interband absorption, meaning that the band gap wavelength must be shifted to longer values. The external voltage in the passive section is zero (unbiased) which corresponds to usual operation conditions

more advanced theory in which further diagrams describing dynamical screening and non diagonal *k*-space dephasing is under development. We hope that it will bring a more accurate description of highly excited semiconductors and can be used to increase further the predictability power of device simulators.

Acknowledgements M. F. Pereira's research is supported by Conselho Nacional de Pesquisas, CNPq of Brazil.

References

[1] R. Zimmermann, Many-Particle Theory of Highly Excited Semiconductors, Teubner Texte zur Physik, Teubner, Leipzig 1987.
[2] M. F. Pereira Jr. and K. Henneberger, Phys. Rev. B **58**, 2064 (1998).
[3] A. Girndt, F. Jahnke, A. Knorr, S. W. Koch, and W. W. Chow, phys. stat. sol. (b) **202**, 725 (1997).
[4] A. Klehr, G. Erbert, J. Sebastian, H. Wenzel, G. Tränkle, and M. F. Pereira Jr., Appl. Phys. Lett. **76**, 2653 (2000).
[5] M. F. Pereira Jr., A. A. Bernussi, W. Carvalho Jr., M. T. Furtado, and A. L. Gobi, accepted at Braz. J. Phys. (2001).
[6] K. Henneberger and H. Haug, Phys. Rev. B **38**, 9759 (1988).
[7] M. F. Pereira Jr. and K. Henneberger, Phys. Rev. B **53**, 16485 (1996).
[8] M. F. Pereira Jr., S. W. Koch, and W. W. Chow, Appl. Phys. Lett. **59**, 2941 (1991).
[9] H. Wenzel, G. Erbert, and P. Enders, IEEE J. Sel. Top. Quantum Electron. **5**, 637 (1999).